REFERENCES AND NOTES

1. G. F. Davies, *J. Geophys. Res.* **89**, 6017 (1984); K. C. Creager and T. H. Jordan, *ibid.* **91**, 3573 (1986); J. Phipps Morgan and P. M. Shearer, *Nature* **365**, 506 (1993).
2. D. P. McKenzie, J. M. Roberts, N. O. Weiss, *J. Fluid Mech.* **62**, 465 (1974); F. M. Richter and D. P. McKenzie, *J. Geophys.* **44**, 441 (1978).
3. C. R. Bina, *Rev. Geophys.* (suppl.) **29** (1991).
4. D. L. Anderson, *J. Geophys. Res.* **92**, 13968 (1987).
5. Other phase effects include latent heat that is either absorbed (endothermic) or released (exothermic) during phase transitions. The effects of latent heat are generally in the sense opposite to that of the local body forces associated with the distortion of phase boundaries [G. Schubert, D. A. Yuen, D. L. Turcotte, *Geophys. J. R. Astron. Soc.* **42**, 705 (1975)]. However, the dynamic effects of latent heat and other phase effects are usually much smaller than the buoyancy force induced by phase-boundary distortion (*12*).
6. Although multiple phase boundaries were considered in (*13*) and some follow-up studies [(*18*); S. Honda, D. A. Yuen, S. Balachandar, D. Reuteler, *Science* **259**, 1308 (1993)], a number of errors in the implementation of phase effects, including the limiting of the phase-related body forces to the phase boundary, prevented significant asymmetric phase effects from being seen.
7. R. Bohler and A. Chopelas, *Geophys. Res. Lett.* **18**, 1147 (1991).
8. T. Kato and M. Kumazawa, in *Dynamic Processes of Material Transformation in the Earth's Interior*, M. Marumo, Ed. (Terra, Tokyo, 1990), pp. 277–208.
9. Y. Fei, S. K. Saxena, A. Navrotsky, *J. Geophys. Res.* **95**, 6915 (1990).
10. A. E. Ringwood, in *The Earth, Its Origin, Structure and Evolution*, M. W. McElhinny, Ed. (Academic Press, New York, 1979), pp. 1–58.
11. M. Liu and C. G. Chase, *J. Geophys. Res.* **94**, 5571 (1989); M. McNutt, *Geophys. Monogr. Am. Geophys. Union* **43**, 1 (1987).
12. U. R. Christensen and D. A. Yuen, *J. Geophys. Res.* **90**, 10291 (1985).
13. M. Liu, D. A. Yuen, W. Zhao, S. Honda, *Science* **252**, 1836 (1991).
14. P. Machetel and P. Weber, *Nature* **350**, 55 (1991); L. P. Solheim and W. R. Peltier, *Can. J. Earth Sci.* **30**, 881 (1993).
15. C. W. Wicks Jr. and M. A. Richards, *Science* **261**, 1424 (1993).
16. G. T. Jarvis and D. P. McKenzie, *J. Fluid Mech.* **96**, 515 (1980).
17. S. A. Weinstein, P. L. Olson, D. A. Yuen, *Geophys. Astrophys. Fluid Dyn.* **47**, 157 (1989).
18. W. L. Zhao, D. A. Yuen, S. Honda, *Phys. Earth Planet. Inter.* **72**, 185 (1992).
19. E. Ito and E. Takahashi, *J. Geophys. Res.* **94**, 10637 (1989).
20. S. Honda and D. A. Yuen, *Earth Planet. Sci. Lett.* **96**, 349 (1990).
21. P. J. Tackley, D. J. Stevenson, G. A. Glatzmaier, G. Schubert, *Nature* **361**, 699 (1993).
22. D. L. Anderson and J. Bass, *ibid.* **320**, 321 (1986); R. Jeanloz and E. Knittle, *Philos. Trans. R. Soc. London Ser. A* **328**, 417 (1989).
23. B. H. Hager and M. A. Richards, *Philos. Trans. R. Soc. London Ser. A* **328**, 309 (1989).

24. Supported by the Research Board of the University of Missouri. I thank C. Chase, J. Engeln, and P. Nabelek for reading an early version of the manuscript.

8 February 1994; accepted 10 May 1994

African *Homo erectus*: Old Radiometric Ages and Young Oldowan Assemblages in the Middle Awash Valley, Ethiopia

J. D. Clark,* J. de Heinzelin, K. D. Schick, W. K. Hart, T. D. White, G. WoldeGabriel, R. C. Walter, G. Suwa, B. Asfaw, E. Vrba, Y. H.-Selassie

Fossils and artifacts recovered from the middle Awash Valley of Ethiopia's Afar depression sample the Middle Pleistocene transition from *Homo erectus* to *Homo sapiens*. Ar/Ar ages, biostratigraphy, and tephrachronology from this area indicate that the Pleistocene Bodo hominid cranium and newer specimens are approximately 0.6 million years old. Only Oldowan chopper and flake assemblages are present in the lower stratigraphic units, but Acheulean bifacial artifacts are consistently prevalent and widespread in directly overlying deposits. This technological transition is related to a shift in sedimentary regime, supporting the hypothesis that Middle Pleistocene Oldowan assemblages represent a behavioral facies of the Acheulean industrial complex.

A *Homo* cranium was found at Bodo, Middle Awash Valley, in Ethiopia's Afar in 1976 (*1*). An age of ~350,000 years for this fossil and stratigraphically associated Acheulean artifacts has been widely assumed based on their morphologies (*2*), but in the absence of radiometric dating. A second hominid's parietal was found in 1981 (BOD-VP-1/1) (*3, 4*) and a distal humerus fragment was recovered in 1990 (BOD-VP-1/2). These specimens straddle the traditional morphological interface between *Homo erectus* and *Homo sapiens*—a transition whose age is poorly defined. The Bodo cranium exhibits cut marks indicating defleshing (*5*). This specimen is usually referred to as "archaic" *Homo sapiens*, as have other inadequately dated specimens from Europe (Arago, Petralona) and Asia (Yunxian).

We recently recovered additional Middle Pleistocene vertebrate fossils at Bodo. In this report, we establish chronostratigraphic control for deposits at Bodo and elucidate the relations between Oldowan and Acheulean assemblages widely distributed in this area. We do not follow a previous stratigraphic framework formulated for the Middle Awash (*6, 7*) because of the difficulty in correlating sedimentary units across a broad region marked by considerable faulting and lacking precise chronometric control. Our fieldwork concentrated on Middle Pleistocene archaeological and paleontological occurrences extending across the modern Bodo, Dawaitoli, and Hargufia catchments (Fig. 1). These are incorporated in fluvial sediments derived from wadis or seasonal rivers on the eastern side of the basin and a major river along the basin axis. These Middle Pleistocene deposits are in fault contact with a sequence of Lower Pleistocene and Pliocene deposits to the east. The Middle Pleistocene deposits are succeeded by a formation exposed as a fault block to the west that bears typical Middle Stone Age artifacts provisionally attributed to the Late Pleistocene.

Most of the in situ Middle Pleistocene deposits in the Bodo-Hargufia area are in a sedimentary unit now informally designated "u" (Fig. 1). This ~35-m-thick package comprises four cyclical sedimentary units and is divided into subunits u1 to u4 (u4 is typically truncated by later erosion). Each subunit consists of gravel sand to clay silt with calcic soils and concretions at the top. Sand and silt of u1 and u2 are indicative of deposition in a stabilized alluvial plain. Those of u3 and u4 reflect increasingly shifting silty overbank and sandy channel deposits. A normal fault (fault 6) to the west separates u1 to u4 from a 15- to 20-m-thick sequence of deposits that appears to represent the continuation of unit u. We informally designate the latter beds as unit u-t. These beds contain abundant Middle Pleistocene vertebrate fossils including the three fossil hominids from the upper Bodo sand unit (UBSU) (*1*). They

J. D. Clark, T. D. White, Y. H.-Selassie, Laboratory for Human Evolutionary Studies, Department of Anthropology, University of California, Berkeley, CA 94720, USA.
J. de Heinzelin, Institut Royal des Sciences Naturelles de Belgique, 1040 Brussels, Belgium.
K. D. Schick, Department of Anthropology, Indiana University, Bloomington, IN 47405, USA.
W. K. Hart, Department of Geology, Miami University, Oxford, OH 45056, USA.
G. WoldeGabriel, EES-1/D462, Los Alamos National Laboratory, Los Alamos, NM 87545, USA.
R. C. Walter, Geochronology Center, Institute of Human Origins, Berkeley, CA 94709, USA.
G. Suwa, Department of Anthropology, University of Tokyo, 113 Tokyo, Japan.
B. Asfaw, Post Office Box 5717, Addis Ababa, Ethiopia.
E. Vrba, Department of Geology and Geophysics, Yale University, New Haven, CT 06511, USA.
*To whom correspondence should be addressed.

also include a number of occurrences of Acheulean artifacts. The UBSU is separated from the top of u1 by at least four sedimentary cycles of unknown duration.

We sampled two different vitric tephra horizons within units u and u-t for Ar/Ar dating (Fig. 1). One of these [MA90-20 (Hargufia) = MA90-7 (Dawaitoli) = MA90-23 (Bodo)] separates u1 and u2 and is correlated on the basis of stratigraphic position, similarities in glass morphology and phenocryst content, and geochemistry (Table 1). This correlation is emphasized by the physical and chemical characteristics of this horizon as compared to other spatially and temporally associated tephra. Samples were dated by the laser-fusion $^{40}Ar/^{39}Ar$ method [following methods described in (8)]. No volcanic horizons were found above the UBSU. We attempted to date tuff MA90-24 from u-t, immediately below the UBSU, but this ash was too contaminated by detrital feldspars. The dated samples MA90-20 and MA90-23 contain small (<0.10 to 0.25 mm) rare potassium feldspars. Although the laser-fusion method is generally well suited for the dating of small grains, the combination of the fine grain size and young age of these feldspars results in significant scatter in the data.

Feldspars from MA90-20 (~0.5 mm) yielded six single grain ages, ranging from 0.51 million years ago (Ma) to 0.73 Ma, and two multiple grain ages of 0.39 Ma and 0.57 Ma. Combined, these data yielded a weighted mean age of 0.55 ± 0.03 Ma (Table 2). A third multiple grain analysis yielded an age of 1.68 Ma, indicating the presence of detrital feldspars. Feldspars from MA90-23 are much more finely grained (<0.25 mm), and we fused three to five grains to increase the precision of the measurement. Five multiple grain ages range from 0.69 to 0.87 Ma and yield a weighted mean age of 0.74 ± 0.03 Ma. (Table 2). The MA90-23 feldspars are compositionally heterogeneous and are consistently older than feldspars from MA90-20. These differences may be due to contamination in the MA90-23 multiple grain analyses.

Pooled together and without the obvious contaminant (L# 4980-09) (Table 2), the MA90-20 and MA90-23 analyses yield a weighted mean age of 0.64 ± 0.03 Ma (Table 2). Such a pooling is justified because an age probability spectrum depicts a normal, Gaussian distribution indicating that these two samples belong to a single age population. Furthermore, an isochron plot of the pooled data yields an age of 0.64 ± 0.04 Ma, an initial $^{40}Ar/^{36}Ar$ intercept of 300 ± 17, and a mean standard weight difference value of 1.6. Taken together, these results indicate that the pooled data fit the criteria for a single age population, with no systematic errors. Given the analytical uncertainty inherent in the measurement of such small, young grains, we believe that the best estimate for the age of this horizon is suggested by the pooled results of 0.64 ± 0.03 Ma. However, the single grain ages from MA90-20 suggest a minimum age of 0.55 ± 0.03 Ma for the base of subunit u2. Overall, these results indicate a temporal correlation with upper members of the Olorgesailie formation in Kenya (Olorgesailie members 10 and 14 are 0.66 Ma and 0.49 Ma, respectively) (9).

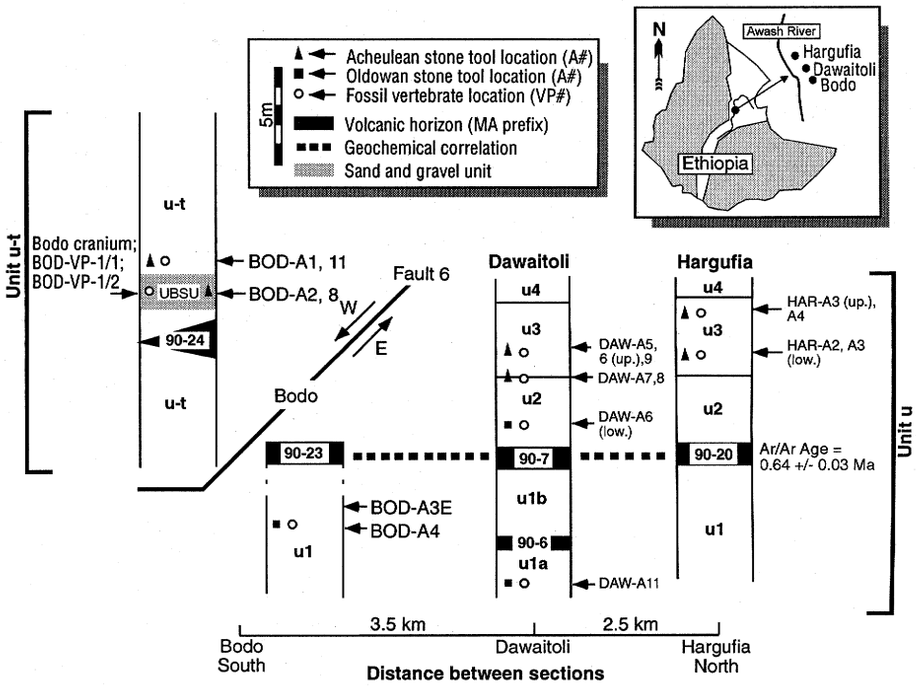

Fig. 1. Stratigraphic relations of Middle Pleistocene deposits (units u and u-t) in the Bodo, Dawaitoli, and Hargufia areas. These deposits are in fault contact with Lower Pleistocene deposits to the east and Upper Pleistocene deposits to the west. Subunit u1 begins with disconformable thick lenses of coarse gravels resulting from the readjustment of the topography to tectonics. Subunit u2 is regularly cyclothemic, with its lower part including a widespread volcanic marker tuff horizon. Peculiar stromatolithic structures occur locally in the middle part of the subunit. Subunit u3 is a variable thickness of valley fills, from fossiliferous sands to silts and clay-silts. Subunit u4 is usually truncated or absent. Sedimentological, structural, archaeological, and biochronological considerations suggest that sequence u-t was emplaced atop unit u before fault 6. Unit u-t and fault 6 are illustrated here only at Bodo, although the same structural relations separate units u and u-t at Dawaitoli and Hargufia.

The archaeological technologies and faunal assemblages from units u and u-t in the Middle Awash are currently indistinguishable and are effectively contemporaneous with similar collections from members 10 and 14 of the Olorgesailie formation. In addition to the Bodo hominids, the paleontological sample from the overlying u-t beds at Bodo yielded excellent cranial material of *Kolpochoerus majus* and *Alcelaphus buselaphus*, *Damaliscus niro*, and *Syncerus acoelotus*. The *Theropithecus oswaldi* and *K. majus* from u and u-t at Bodo (*10*), Dawaitoli, and Hargufia indicate a good biochronological match for Olduvai bed IV and the upper levels at Olorgesailie. The Bodo bovids fit this assessment and are in accord with the Middle Awash radiometric dates.

A distal third of a hominid humerus lacking an articular end (BOD-VP-1/2) was recovered in 1990 from the surface of the upper Bodo sands ~100 m north of the original Bodo cranium discovery. Aside from a greater cortical thickness, this fossil has no morphological features noticeably different from modern human comparative specimens. This new Bodo humerus is appreciably smaller than many modern human humeri. The two other Bodo hominid individuals are represented by large and robust cranial remains recovered from the same locality. The relatively small size of the new humerus may reflect pronounced sexual dimorphism in this hominid form, also suggested by broadly contemporary, smaller cranial remains from other African sites such as Salé and Ndutu. Several workers have identified primitive characters of the Bodo crania that accord well with an older age for the fossils than previously thought (*1*, *3*). However, most workers have identified the Bodo specimen as "archaic" *Homo sapiens* on the basis of its derived morphology compared to typical *Homo erectus* of Java and China.

Our placement of the Bodo cranium at

Table 1. Compositional data for Hargufia-Dawaitoli-Bodo tuffs. See Fig. 1 for geographic and stratigraphic locations. All values are given in parts per million except Fe_2O_3, Al_2O_3, and CaO, which are given as weight percent (*32*).

Location	Fe_2O_3	Al_2O_3	CaO	Ba	Mn	Nb	Rb	Sr	Ti	Y	Zn	Zr
MA90-7	6.06	11.51	0.52	985	1646	119	116	23	2177	99	232	676
MA90-20	6.09	11.62	0.53	985	1701	125	116	18	2241	96	219	659
MA90-23	6.11	11.51	0.56	1001	1743	124	116	21	2278	98	223	663
MA90-6	7.11	10.46	0.43	572	2031	135	100	6	2319	102	256	831
MA90-24	8.79	7.98	0.35	1013	2284	138	96	46	1480	119	301	681

Table 2. Laser-fusion $^{40}Ar/^{39}Ar$ results. The laboratory run number is indicated by L#, the number of grains measured in each fusion is indicated by *n*, and the percent radiation is indicated by % Rad. (*33*). The average and SD of the Ca/U ratio as well as the weighted mean and uncertainty, respectively, are 0.0133, 0.0127, 0.554, and 0.032 for MA90-20 (J = 0.000315 ± 0.000002); 0.2819, 0.4528, 0.739, and 0.028 for MA90-23 (J = 0.0003187 ± 0.000001); and 0.1166, 0.2949, 0.639, and 0.034 in the pooled results (L#4980-01 to L#4980-08 for MA90-20 and L#5005-01 to L#5005-05 for MA90-23). The material was sanidine except for L#5005-03 (Plagioclase) and L#5005-05 (anorthoclase).

L#	*n*	Ca/K	% Rad.	Age (Ma)	± Ma
		MA90-20			
4980-01	1	0.0122	33.8	0.533	0.053
4980-02	1	0.0289	56.6	0.648	0.063
4980-03	1	0.0029	97.6	0.632	0.163
4980-04	1	0.0119	30.0	0.731	0.072
4980-05	1	0.0000	75.8	0.597	0.054
4980-06	1	0.0359	53.9	0.511	0.033
4980-07	3	0.0040	46.3	0.389	0.073
4980-08	3	0.0105	22.8	0.565	0.075
4980-09	3	0.0403	70.1	1.681	0.033
		MA90-23			
5005-01	3	0.0536	79.1	0.701	0.044
5005-02	3	0.0062	65.5	0.687	0.046
5005-03	3	1.0680	89.3	0.871	0.080
5005-04	3	0.0102	94.6	0.776	0.043
5005-05	5	0.2717	46.6	0.748	0.047

~0.6 Ma is based on the structural, biostratigraphic, and archaeological considerations outlined above. These tie the fossils to the adjacent unit u, whose best age is 0.64 ± 0.04 Ma and whose minimum age is 0.55 ± 0.03 Ma. This placement has significant implications for the interpretation of hominid evolution across the Middle Pleistocene. Age estimates for south and east Asian representatives of *Homo erectus* overlap the Bodo age estimate (*11*, *12*). If these estimates for Asian fossils are correct, evolution within African and Asian *Homo erectus* may have followed different trajectories, with advanced features appearing earlier in Africa (*13*–*15*). Alternatively, other specimens interpreted to have evolved from *Homo erectus* (such as Arago, Petralona, and Yunxian) may be substantially older than generally thought (~0.5 Ma rather than 0.3 Ma).

Artifacts were excavated at HAR-A4 and DAW-A6 and found eroding from individual horizons at various localities in the three modern drainages. Assemblages in u1 and u2 consist of simple cores and flakes typical of Oldowan technology; bifaces are notably absent. Flakes are predominantly cortical or plain-platformed, primarily unmodified, with rare, minimal retouch. Five pairs of conjoining flakes were found at BOD-A3. In contrast, Acheulean artifacts dominated by relatively well made, bifacial hand axes and cleavers first become abundant in subunit u3 and above, consistently found eroding from alluvial sediments associated with shallow channels or channel banks. Oldowan and Acheulean artifacts are mostly in a fresh, unabraded condition. The HAR-A4 (in u3) excavations yielded a small number of bifaces in situ as well as a large number of flakes and flake fragments, a significant proportion of which were quite small (1 to 2 cm in maximum dimension). These relations indicate that sorting before burial was minimal.

The local shift from Oldowan to Acheulean assemblages observed in the Middle Awash comes substantially later than the appearance of the Acheulean in Africa, dated elsewhere minimally at 1.5 Ma (*16*). Oldowan and Acheulean assemblages found in contemporary Olduvai bed II deposits were attributed first to different contemporary hominid taxa (*17*) and then to different technological responses to different habitat (*18*–*20*) or raw material use (*21*). The local Middle Awash assemblage change comes within unit u; there is no faunal difference between the Oldowan levels (u1 and u2) and the overlying unit in which Acheulean artifacts become pervasive (u3). There is, however, a progressive change in the sedimentary regime: The wadi fan environment became increasingly dominant, and sands accounted for a greater volume of the section in subunit u3. The Middle Awash change from core (chopper)-based Oldowan assemblages to assemblages with large quantities of Acheulean bifaces appears to reflect the use of different technologies in different geographic settings. Isaac (*22*) noted the clustering of Acheulean tools in areas with a sandy substratum, suggesting mechanisms of hominid preference and hydraulic agency to account for this observation (*23*). The Middle Awash data are consistent with such interpretations. Future use of the landscape approach to interpret archaeological assemblages (*24*, *25*) will explore late Oldowan assemblages as activity facies of the Acheulean (*26*).

Older radiometric ages (0.64 Ma) for the Middle Awash and for upper Olorgesailie (0.6 to 0.74 Ma) (*9*) combine with the discovery of much older (1.0 to 1.5 Ma) Acheulean occurrences at Konso-Gardula (*16*), Kesem-Kebena (*27*), and Bouri (*28*) to emphasize the long duration of the Acheulean. These findings couple with new evidence for possible early (1.6 to 1.8 Ma) hominid occupation of Java (*29*) to show that the Old World origins, dispersal, culture, and evolution of *Homo erectus* were very complex.

REFERENCES AND NOTES

1. G. C. Conroy, C. J. Jolly, D. Cramer, J. Kalb, *Nature* **275**, 67 (1978).
2. G. Brauer and E. J. Mbua, *J. Hum. Evol.* **22**, 79 (1992).
3. B. Asfaw, *Am. J. Phys. Anthropol.* **61**, 367 (1983).
4. J. D. Clark *et al.*, *Nature* **307**, 423 (1984).
5. T. White, *Am. J. Phys. Anthropol.* **69**, 503 (1986).
6. J. E. Kalb *et al.*, *Nature* **298**, 17 (1982).
7. J. E. Kalb, E. B. Oswald, A. Mebrate, S. Tebedge, C. J. Jolly, *Newsl. Stratigr.* **11**, 95 (1982).
8. R. C. Walter, P. C. Manega, R. L. Hay, R. E. Drake, G. H. Curtis, *Nature* **354**, 145 (1991).
9. A. Deino and R. Potts, *J. Geophys. Res.* **95**, 8453 (1990).
10. J. E. Kalb *et al.*, *Nature* **298**, 25 (1982).
11. J. S. Aigner, *Anthropos (Brno)* **23**, 157 (1986).
12. M. Zhou and C. K. Ho, *Geol. Soc. Am. Spec. Pap. 242* (1990), p. 69.
13. P. Andrews, *Cour. Forsch. Inst. Senckenberg* **69**, 167 (1984).
14. R. J. Clarke, *J. Hum. Evol.* **19**, 699 (1990).
15. G. P. Rightmire, *The Evolution of* Homo erectus (Cambridge Univ. Press, New York, 1990).
16. B. Asfaw *et al.*, *Nature* **360**, 732 (1992).
17. M. D. Leakey, *Excavations in Beds I and II, 1960–1963*, vol. 3 of *Olduvai Gorge* (Cambridge Univ. Press, Cambridge, 1971).
18. J. D. Clark, *The Prehistory of Africa* (Praeger, New York, 1970).
19. ———, in *After the Australopithecines*, G. Ll. Isaac and K. Butzer, Eds. (Mouton, The Hague, Netherlands, 1975), pp. 608–611.
20. R. L. Hay, *Geology of the Olduvai Gorge* (Univ. of California Press, Berkeley, 1976).
21. D. Stiles, *Afr. Archaeol. Rev.* **9**, 1 (1991).
22. G. Ll. Isaac, *Publ. Mus. Arqueol.* (5th Panafrican Congress, Santa Cruz de Tenerife, Spain) **6** (2), 135 (1966).
23. ———, *Olorgesailie: Archaeological Studies of a Middle Pleistocene Lake Basin in Kenya* (Univ. of Chicago Press, Chicago, 1977).
24. R. Potts, *J. Hum. Evol.* **18**, 477 (1989).
25. R. Blumenschine, *ibid.* **21**, 451 (1991).
26. J. A. J. Gowlett, *World Archaeol.* **20**, 13 (1988).
27. G. WoldeGabriel *et al.*, *J. Field Archaeol.* **19**, 471 (1992).
28. Middle Awash project work at Bouri in 1992 has yielded large collections of vertebrate (including hominid) and archaeological remains that obviously antedate the Bodo assemblages on biochronological grounds, as predicted in (*4*).
29. C. C. Swisher III *et al.*, *Science* **263**, 1118 (1994).
30. A. Deino, L. Tauxe, M. Monaghan, R. J. Drake, *J. Geol.* **98**, 567 (1990).
31. S. D. Samson and E. C. Alexander, *Chem. Geol. (Isotope Geosci. Sect.)* **66**, 27 (1987).
32. All analyses were by direct-current argon plasma spectrometry on pure bulk glass separates. The

glass in samples MA90-7, MA90-20, and MA90-23 contained significant feldspar microlites. To insure that only pure glass (>99%) was analyzed, a special procedure was developed to separate even finely disseminated impurities from the glass. The final purity was determined by the inspection of powdered bulk glass separates (<325 mesh; 45 μm) with transmitted light microscopy and by comparison of the DCP bulk glass Fe, Ca, Al, Mn, and Ti concentrations with those determined by grain discrete electron microprobe analyses. These steps were applied to all samples of this study to facilitate comparisons and correlations. Concentrations of Fe, Ca, Al, Mn, and Ti were determined by comparison of unknown intensities to calibration curves on the basis of six internationally recognized rock standards. All other concentrations were determined by the method of standards addition with the use of a multi-element spike solution designed specifically for silicic compositions.

33. The Ca/K ratio is derived by the multiplication of the measured $^{37}Ar/^{39}Ar$ ratio by 1.96. The weighted mean age and error (∂; 1 sigma) are computed with an inverse variance weighting factor that uses deviations about a weighted mean to determine the weighted error (*30, 31*). Individual grain errors reflect errors in the fluence monitor constant (J) and in the determination of Ar isotopic ratios, which in turn propagate errors in discrimination and in Ar beam intensities from sample and blank (*30*). The data in italics are excluded from the mean age. Feldspars were irradiated for 0.5 hour at 8 MW at the Omega West research reactor of the Los Alamos National Laboratory, which has a fast neutron fluence of 5.7 × 1013 neutrons per centimeter per second. Cadmium shielding was used to reduce the thermal neutron production of ^{40}Ar. After irradiation, the samples were transferred to a copper holder and loaded onto the extraction line for overnight bakeout at ~200°C. Samples were fused with an 8-W argon-ion laser (Mass Analyser Products, Nottingham, United Kingdom). Abundances of the argon isotopes were measured on a MAP-215 noble gas spectrometer fitted with a Balzers electron multiplier operating at a gain of about 20,000. Typical system blank volumes of ^{40}Ar, ^{39}Ar, ^{38}Ar, ^{37}Ar, and ^{36}Ar are 4, 2, 0.08, 0.3, and 0.3 × 10^{-17} mol, respectively. Sanidine from the Fish Canyon tuff was used as the neutron fluence monitor, which has a reference age of 27.84 Ma (*30*). The constants used in this study are as follows: $(\lambda_\epsilon + \lambda_\epsilon' = 0.581 \times 10^{-10}$/year; $\lambda_\beta = 4.962 \times 10^{10}$/year; 40 K per degree kelvin = 1.167×10^{-4} mol/mol).

34. We thank the National Science Foundation, the National Geographic Society, the Japan Society for the Promotion of Science, the University of California Collaborative Research Program of the Institute of Geophysics and Planetary Physics at Los Alamos National Laboratory, the Ethiopian Ministry of Culture and Sports Affairs, the National Museum of Ethiopia, the Afar people, A. Ademassu, B. Latimer, S. Yirga, G. Hundie, A. Negash, Z. Assefa, and C. Tilahun for making the 1990 Middle Awash research possible. We also thank F. C. Howell and B. Dalrymple for helpful suggestions on the paper.

8 February 1994; accepted 2 May 1994

MCM-22: A Molecular Sieve with Two Independent Multidimensional Channel Systems

Michael E. Leonowicz, Jeffrey A. Lawton,* Stephen L. Lawton,† Mae K. Rubin

The molecular sieve MCM-22 contains structural features previously unobserved in this class of materials. Its framework topology, derived from high-resolution electron micrographs and refined with synchrotron x-ray diffraction powder data, contains two independent pore systems, both of which are accessed through rings composed of ten tetrahedral (T) atoms (such as Si, Al, and B). One of these pore systems is defined by two-dimensional, sinusoidal channels. The other consists of large supercages whose inner free diameter, 7.1 angstroms, is defined by 12 T–O species (12-rings) and whose inner height is 18.2 angstroms. These coexisting pore systems may provide opportunities for a wide variety of catalytic applications in the petrochemical and refining industries. Another structural feature is an unusual -T-O-T- chain that passes through the center of a modified dodecasil-1H [$4^3 5^6 6^3$] cage.

Molecular sieves are crystalline, microporous materials with frameworks of tetrahedral atoms that are interconnected in three dimensions through oxygen atoms. Their pore structure makes them useful in the petrochemical and refining industries for catalysis and separation processes. Synthesis is usually carried out under hydrothermal conditions. A directing agent, if present in the reaction gel, may be used to influence the formation and geometry of the internal pore system. The molecular sieve MCM-22 was synthesized in this manner, with hexahydro-1H-azepine (hexamethyleneimine) as a directing agent. We propose a model for the structure of this molecular sieve.

MCM-22 may be synthesized as an aluminosilicate or borosilicate. Scanning electron micrographs revealed that it crystallizes as very thin sheets and that boron MCM-22 crystallites are typically thicker than those from aluminum syntheses. Boron-containing samples were chosen for structural studies because their large size gave rise to powder x-ray diffraction (XRD) patterns with sharper peaks.

The MCM-22 sample used in this study was hydrothermally synthesized by procedures described elsewhere (*1*) from Hi-Sil precipitated silica (87% SiO_2), hexamethyleneimine (HMI), triethanolamine, boric acid (H_3BO_3), and sodium hydroxide (50% NaOH solution). Triethanolamine (320 g) was added to a solution containing 14.0 g of H_3BO_3, 6.3 g of NaOH, and 160 g of H_2O; 96.0 g of Hi-Sil were then added, followed by 42.0 g of HMI. After vigorous stirring for 1 hour, 100 g of this slurry were transferred to a Teflon-lined stainless steel autoclave. The vessel was placed in an oil bath, and the reaction mixture was crystallized under static conditions at 120°C for 230 days. The solid product was washed with water and dried overnight at 120°C (*2*) and then calcined in air at 540°C for 16 hours. This calcined product, $H_{0.033}Na_{0.043}(Al_{0.005}B_{0.071}Si_{0.924})O_2$, is referred to as MCM-22.

Electron diffraction (ED) photographs indicated that the unit cell had hexagonal symmetry with no systematic absences. They exhibited Laue symmetry consistent with the eight hexagonal space groups *P6/mmm*, *P$\bar{6}$2m*, *P$\bar{6}$m2*, *P6mm*, *P622*, *P$\bar{3}$1m*, *P31m*, and *P312*. The XRD data for the structure refinement of the calcined sample were collected on beamline X7A at the National Synchrotron Light Source in Brookhaven National Laboratory (*3*). These data were successfully indexed on a hexagonal lattice and were fully consistent with a space group that exhibits no systematic extinctions. The refined unit cell parameters were a = 14.1145(8) Å and c = 24.8822(18) Å (*4*).

The structure was determined with high-resolution electron micrograph (HREM) lattice images and model building. Trial models were refined by the program DLS (*5*), and the model whose calculated XRD pattern most closely resembled the experimental pattern was subjected to a Rietveld refinement (*6*) (Fig. 1). Final atomic coordinates are given in Table 1. There are 72 T atoms per unit cell.

As seen in projections of the framework topology for MCM-22 (Figs. 2 and 3), the [001] projection is remarkably similar to that of the silica clathrate dodecasil-1H (DOH) (*7*) (Fig. 3). Topologically, the two framework connectivities are related. The DOH structure contains hexagonal sheets of [$4^3 5^6 6^3$] cages (*8*) (Fig. 4A) that share 4-ring faces with adjacent cages within the sheet. Large 12-ring cavities bordered by six joined cages are created within these sheets. These sheets, in turn, join along the unit cell c direction through single 6-rings that cap the 12-ring cavities at either end, giving the cavity [$6^8 5^{12}$] topology. Adjacent sheets are also directly connected through bonds between apical T atoms on the threefold axes of [$4^3 5^6 6^3$] cages.

Mobil Research and Development Corporation, P.O. Box 480, Paulsboro, NJ 08066, USA.

*Present address: Program in Cell and Molecular Biology, Baylor College of Medicine, One Baylor Plaza, Houston, TX 77030, USA.

†To whom correspondence should be addressed.